UMN-D-01-7
OHSTPY-HEP-T-01-016
hep-th/0106193

Wave functions and properties of massive states in three-dimensional supersymmetric Yang–Mills theory

John R. Hiller
Department of Physics, University of Minnesota Duluth, Duluth, MN 55812

Stephen Pinsky and Uwe Trittmann
Department of Physics, The Ohio State University, Columbus, OH 43210
(June 4, 2005)

Abstract

We apply supersymmetric discrete light-cone quantization (SDLCQ) to the study of supersymmetric Yang–Mills theory on $\mathbf{R} \times S^1 \times S^1$. One of the compact directions is chosen to be light-like and the other to be space-like. Since the SDLCQ regularization explicitly preserves supersymmetry, this theory is totally finite, and thus we can solve for bound-state wave functions and masses numerically without renormalizing. We present an overview of all the massive states of this theory, and we see that the spectrum divides into two distinct and disjoint sectors. In one sector the SDLCQ approximation is only valid up to intermediate coupling. There we find a well defined and well behaved set of states, and we present a detailed analysis of these states and their properties. In the other sector, which contains a completely different set of states, we present a much more limited analysis for strong coupling only. We find that, while these state have a well defined spectrum, their masses grow with the transverse momentum cutoff. We present an overview of these states and their properties.

I. INTRODUCTION

The properties of strongly coupled gauge theories with a sufficient amount of supersymmetry can be analyzed in great detail [1–3]. In particular, there are a number of supersymmetric gauge theories that are believed to be interconnected through a web of strong-weak coupling dualities. While these dualities provide a great deal of insight, there is still a need to study the bound states of these theories directly and at any coupling.

It is well known that (1+1)-dimensional field theories *can* be solved from first principles via a straightforward application of discrete light-cone quantization (DLCQ) [4,5]. This includes a large class of supersymmetric gauge theories in two dimensions. More recently a supersymmetric form of DLCQ (or 'SDLCQ'), which is known to preserve supersymmetry, has been developed [6–12]. We have recently shown that the SDLCQ algorithms can be extended to solve higher-dimensional theories [13]. One important difference between two-dimensional and higher-dimensional theories is the phase diagram induced by variations in the gauge coupling. The spectrum of a (1+1)-dimensional gauge theory scales trivially with respect to the gauge coupling, while a theory in higher dimensions has the potential of exhibiting a complex phase structure, which may include strong, intermediate, and weak coupling regions [13]. It is therefore interesting to study the properties of the bound states of gauge theories in $D \geq 3$ dimensions in all of these regions.

Towards this end, we apply SDLCQ to the study of three-dimensional SU(N_c) $\mathcal{N} = 1$ super-Yang–Mills theory compactified on the space-time $\mathbf{R} \times S^1 \times S^1$. This extends previous work [13,14] to better numerical resolution and includes extraction of wave functions for bound states at these higher resolutions. We work in the large-N_c limit, with the light-cone coordinate x^- and transverse spatial coordinate $x_\perp$ compactified on the circles S^1. As is customary in DLCQ, we drop the longitudinal zero modes [6–9,11,13,15–18]. A review of dynamical and constrained zero modes can be found in [5].

We are able to solve for bound states and their properties numerically by diagonalizing the discretized light-cone supercharge. Since we do not break the supersymmetry, the resulting spectrum is exactly supersymmetric. Study of the entire spectrum, which one obtains by a complete diagonalization of the entire Hamiltonian, shows that the spectrum breaks up into three distinct parts, which we will call the weak, intermediate, and strong-coupling regions. The weak-coupling region is closely related to the dimensionally reduced theory, and we have discussed it elsewhere [13]. By the intermediate-coupling region, we refer to the low-mass portion of the spectrum. We will see that this region clearly separates from the high-mass region for couplings beyond weak coupling. We will also see that a standard DLCQ analysis of these low-mass states is only possible at intermediate coupling. We will present a detailed analysis of these states and their properties in this region. We then look at the high-mass spectrum and show that it appears to behave as a strongly coupled spectrum. Unfortunately, a detailed analysis of these states requires a complete diagonalization of the Hamiltonian and that is beyond the scope of this work.

The remainder of the paper is structured as follows. In Sec. II, we summarize the formulation of SU(N_c) $\mathcal{N} = 1$ super-Yang–Mills theory defined on the compactified space-time $\mathbf{R} \times S^1 \times S^1$. This includes explicit expressions for the light-cone supercharges and their discretization via SDLCQ. Also discussed are discrete symmetries of the theory that are helpful in classifying the spectrum. In Sec. III, we discuss the numerical methods that we use and present an overview of the full spectrum of the theory. In Sec. IV, we present a detailed analysis of the states in the low-mass sector, where the SDLCQ approximation is only valid up to intermediate coupling. This includes a study of the convergence of the states in both transverse and longitudinal resolutions. We present some of the properties of these states and calculate transverse-momentum distribution functions for some of these states. In Sec. V, we consider the other distinct sector of states. We present the scaled mass spectrum as a function of the inverse coupling and discuss the strong-coupling spectrum as

a function of the transverse momentum cutoff. In Sec. VI, we conclude by discussing the general properties of this theory and their implications.

II. LIGHT-CONE QUANTIZATION AND SDLCQ

The action for three-dimensional $\mathcal{N}=1$ supersymmetric Yang–Mills theory, in a space-time compactified on a scale L in the transverse direction $x_\perp = x^2$, is

$$S = \int d^2x \int_0^L dx_\perp \mathrm{tr}(-\frac{1}{4}F^{\mu\nu}F_{\mu\nu} + \mathrm{i}\bar{\Psi}\gamma^\mu D_\mu \Psi)\,, \tag{2.1}$$

where A_μ and Ψ are traceless $N_c \times N_c$ hermitian matrices transforming in the adjoint representation of $SU(N_c)$, and we suppress color indices. We introduce light-cone coordinates $x^\pm = (x^0 \pm x^1)/\sqrt{2}$ and choose to work in the light-cone gauge $A^+ = 0$. With chiral projections of the spinor Ψ defined by

$$\psi = \frac{1+\gamma^5}{2^{1/4}}\Psi\,, \qquad \chi = \frac{1-\gamma^5}{2^{1/4}}\Psi\,, \tag{2.2}$$

and $\phi \equiv A^2$, the action becomes

$$S = \int dx^+dx^- \int_0^L dx_\perp \mathrm{tr}\left[\frac{1}{2}(\partial_- A^-)^2 + (D_+\phi + \partial_\perp A^-)\partial_-\phi + \mathrm{i}\psi D_+\psi + \right.$$
$$\left. + \mathrm{i}\chi\partial_-\chi + \frac{\mathrm{i}}{\sqrt{2}}\psi D_\perp \chi + \frac{\mathrm{i}}{\sqrt{2}}\chi D_\perp \psi\right]\,. \tag{2.3}$$

We choose the light-cone gauge because the non-dynamical fields A^- and χ may be obtained explicitly from their equations of motion, which are actually constraint equations in light-cone coordinates. These fields are then given in terms of the physical degrees of freedom ϕ and ψ as

$$A^- = \frac{1}{\partial_-^2}J = \frac{1}{\partial_-^2}\left(ig[\phi,\partial_-\phi] + 2g\psi\psi - \partial_\perp\partial\phi\right)\,, \quad \chi = -\frac{1}{\sqrt{2}\partial_-}D_\perp\psi\,. \tag{2.4}$$

The light-cone energy P^- and momentum operators, P^+ and $P^\perp$, become

$$P^+ = \int dx^- \int_0^L dx_\perp \mathrm{tr}\left[(\partial_-\phi)^2 + \mathrm{i}\psi\partial_-\psi\right]\,, \tag{2.5}$$

$$P^- = \int dx^- \int_0^L dx_\perp \mathrm{tr}\left[-\frac{1}{2}J\frac{1}{\partial_-^2}J - \frac{\mathrm{i}}{2}D_\perp\psi\frac{1}{\partial_-}D_\perp\psi\right]\,, \tag{2.6}$$

$$P^\perp = \int dx^- \int_0^L dx_\perp \mathrm{tr}\left[\partial_-\phi\partial_\perp\phi + \mathrm{i}\psi\partial_\perp\psi\right]\,. \tag{2.7}$$

The chiral projections of the light-cone supercharge, a two-component Majorana spinor, are

$$Q^+ = 2^{1/4}\int dx^- \int_0^L dx_\perp \mathrm{tr}\left[\phi\partial_-\psi - \psi\partial_-\phi\right]\,, \tag{2.8}$$

$$Q^- = 2^{3/4}\int dx^- \int_0^L dx_\perp \mathrm{tr}\left[\partial_\perp\phi\psi + g\left(\mathrm{i}[\phi,\partial_-\phi] + 2\psi\psi\right)\frac{1}{\partial_-}\psi\right]\,. \tag{2.9}$$

At large N_c the canonical (anti-)commutators for the propagating fields are, at equal light-cone time x^+,

$$\Big[\phi_{ij}(x^-,x_\perp),\partial_-\phi_{kl}(y^-,y_\perp)\Big]=\Big\{\psi_{ij}(x^-,x_\perp),\psi_{kl}(y^-,y_\perp)\Big\}=\frac{1}{2}\delta(x^--y^-)\delta(x_\perp-y_\perp)\delta_{il}\delta_{jk}\,. \tag{2.10}$$

From these one can derive the supersymmetry algebra

$$\{Q^+,Q^+\}=2\sqrt{2}P^+,\qquad \{Q^-,Q^-\}=2\sqrt{2}P^-,\qquad \{Q^+,Q^-\}=-4P_\perp\,. \tag{2.11}$$

We will only consider the sector where the total transverse momentum is zero. The other allowed sectors, given our compactification, have transverse momentum $2\pi n/L$, with n a nonzero integer. In the sector with zero transverse momentum, Q^+ and Q^- anticommute with each other, and the supersymmetry algebra is equivalent to the $\mathcal{N}=(1,1)$ supersymmetry of the two-dimensional theory obtained by dimensional reduction [6]. Also in this sector, the mass squared operator is given by $2P^+P^-$. The eigenvalue problem for the bound states is then $2P^+P^-|M\rangle=M^2|M\rangle$, with $|M\rangle$ expanded in a Fock basis diagonal in P^+ and $P^\perp$.

The expansions of the field operators in terms of creation and annihilation operators for the Fock basis are

$$\begin{aligned}
&\phi_{ij}(0,x^-,x_\perp)=\\
&\qquad\frac{1}{\sqrt{2\pi L}}\sum_{n^\perp=-\infty}^{\infty}\int_0^\infty\frac{dk^+}{\sqrt{2k^+}}\left[a_{ij}(k^+,n^\perp)e^{-\mathrm{i}k^+x^-+\mathrm{i}\frac{2\pi n^\perp}{L}x_\perp}+a^\dagger_{ji}(k^+,n^\perp)e^{\mathrm{i}k^+x^--\mathrm{i}\frac{2\pi n^\perp}{L}x_\perp}\right],\\
&\psi_{ij}(0,x^-,x_\perp)=\\
&\qquad\frac{1}{2\sqrt{\pi L}}\sum_{n^\perp=-\infty}^{\infty}\int_0^\infty dk^+\left[b_{ij}(k^+,n^\perp)e^{-\mathrm{i}k^+x^-+\mathrm{i}\frac{2\pi n^\perp}{L}x_\perp}+b^\dagger_{ji}(k^+,n^\perp)e^{\mathrm{i}k^+x^--\mathrm{i}\frac{2\pi n^\perp}{L}x_\perp}\right].
\end{aligned}$$

From the field (anti-)commutators one finds

$$\Big[a_{ij}(p^+,n_\perp),a^\dagger_{lk}(q^+,m_\perp)\Big]=\Big\{b_{ij}(p^+,n_\perp),b^\dagger_{lk}(q^+,m_\perp)\Big\}=\delta(p^+-q^+)\delta_{n_\perp,m_\perp}\delta_{il}\delta_{jk}\,. \tag{2.12}$$

Notice that the compactification in $x^\perp$ means that the transverse momentum modes are summed over a discrete set of values $2\pi n^\perp/L$. In order to have a finite matrix representation for the eigenvalue problem, we must truncate these sums at some fixed integers $\pm T$. The value of T defines a physical transverse cutoff $\Lambda_\perp=2\pi T/L$; however, given this definition, T can also be viewed as a measure of transverse resolution at fixed $\Lambda_\perp$.

The supercharges take the following forms:

$$Q^+=\mathrm{i}2^{1/4}\sum_{n^\perp\in\mathbf{Z}}\int_0^\infty dk\sqrt{k}\left[b^\dagger_{ij}(k,n^\perp)a_{ij}(k,n^\perp)-a^\dagger_{ij}(k,n^\perp)b_{ij}(k,n^\perp)\right], \tag{2.13}$$

$$Q^-=\frac{2^{7/4}\pi\mathrm{i}}{L}\sum_{n^\perp\in\mathbf{Z}}\int_0^\infty dk\frac{n^\perp}{\sqrt{k}}\left[a^\dagger_{ij}(k,n^\perp)b_{ij}(k,n^\perp)-b^\dagger_{ij}(k,n^\perp)a_{ij}(k,n^\perp)\right]+$$

$$
\begin{aligned}
&+\frac{\mathrm{i}2^{-1/4}g}{\sqrt{L\pi}}\sum_{n_i^\perp\in\mathbf{Z}}\int_0^\infty dk_1dk_2dk_3\delta(k_1+k_2-k_3)\delta_{n_1^\perp+n_2^\perp,n_3^\perp}\\
&\times\left\{\frac{1}{2\sqrt{k_1k_2}}\frac{k_2-k_1}{k_3}[a_{ik}^\dagger(k_1,n_1^\perp)a_{kj}^\dagger(k_2,n_2^\perp)b_{ij}(k_3,n_3^\perp)-b_{ij}^\dagger(k_3,n_3^\perp)a_{ik}(k_1,n_1^\perp)a_{kj}(k_2,n_2^\perp)]\right.\\
&+\frac{1}{2\sqrt{k_1k_3}}\frac{k_1+k_3}{k_2}[a_{ik}^\dagger(k_3,n_3^\perp)a_{kj}(k_1,n_1^\perp)b_{ij}(k_2,n_2^\perp)-a_{ik}^\dagger(k_1,n_1^\perp)b_{kj}^\dagger(k_2,n_2^\perp)a_{ij}(k_3,n_3^\perp)]\\
&+\frac{1}{2\sqrt{k_2k_3}}\frac{k_2+k_3}{k_1}[b_{ik}^\dagger(k_1,n_1^\perp)a_{kj}^\dagger(k_2,n_2^\perp)a_{ij}(k_3,n_3^\perp)-a_{ij}^\dagger(k_3,n_3^\perp)b_{ik}(k_1)a_{kj}(k_2,n_2^\perp)]\\
&\left.+(\frac{1}{k_1}+\frac{1}{k_2}-\frac{1}{k_3})[b_{ik}^\dagger(k_1,n_1^\perp)b_{kj}^\dagger(k_2,n_2^\perp)b_{ij}(k_3,n_3^\perp)+b_{ij}^\dagger(k_3,n_3^\perp)b_{ik}(k_1,n_1^\perp)b_{kj}(k_2,n_2^\perp)]\right\}.
\end{aligned}
\tag{2.14}
$$

All sums over the transverse momentum indices are truncated at $\pm T$. The symmetric truncation with respect to positive and negative modes aids in retaining a reflection parity symmetry in the states.

The remaining step of the (S)DLCQ procedure [6,12,13] is discretization in the longitudinal direction. This is equivalent to the choice of periodic boundary conditions in x^- [19]. For a review of ordinary DLCQ, see [5]. Where DLCQ and SDLCQ differ is in the construction of the discrete P^-. In DLCQ this is done directly, but in SDLCQ it is the supercharge that is discretized, with P^- constructed from the anticommutator of Q^- in the supersymmetry algebra. The difference between the two discretizations disappears in the continuum limit. The advantage of the SDLCQ approach is that the spectrum obtained from its discrete P^- is explicitly supersymmetric at any numerical resolution, whereas the DLCQ spectrum becomes supersymmetric only in the continuum limit. For additional discussion of this point, see Ref. [14]. The specifics of the longitudinal discretization are presented in the following section on numerical methods.

The spectrum can be classified according to three commuting Z_2 symmetries of Q^-. As described in [14], they are transverse parity

$$
P: a_{ij}(k,n^\perp)\to -a_{ij}(k,-n^\perp)\,,\qquad b_{ij}(k,n^\perp)\to b_{ij}(k,-n^\perp)\,;
\tag{2.15}
$$

the T symmetry defined by Kutasov [18], which we call S symmetry, to avoid confusion with the transverse cutoff T,

$$
S: a_{ij}(k,n^\perp)\to -a_{ji}(k,n^\perp)\,,\qquad b_{ij}(k,n^\perp)\to -b_{ji}(k,n^\perp)\,;
\tag{2.16}
$$

and the product of these two symmetries, $R=PS$. We diagonalize the supercharge separately in the four sectors defined by the four possible combinations of P and S eigenvalues. This significantly reduces the size of the individual matrices required for a given level of resolution. The P symmetry is associated with a double degeneracy of the massive states, that is in addition to the usual boson/fermion degeneracy of supersymmetry. A demonstration of this is given in [14].

III. NUMERICAL METHODS

We convert the mass eigenvalue problem $2P^+P^-|M\rangle = M^2|M\rangle$ to a matrix eigenvalue problem by introducing a discrete P^- in a basis where P^+ and $P^\perp = 0$ are diagonal. As discussed in the previous section, this is done in SDLCQ by first discretizing the supercharge Q^- and then constructing P^- from the square of the supercharge: $P^- = (Q^-)^2/\sqrt{2}$. We have already introduced a finite discretization in the transverse direction, characterized by the compactification scale L and cutoff or resolution T. To complete the discretization of the supercharge, we introduce discrete longitudinal momenta k^+ as fractions nP^+/K of the total longitudinal momentum P^+. Here $n < K$ and K are positive integers. It is in the nature of light-cone coordinates that the longitudinal momenta can be chosen positive, and that n and the number of partons are bounded by K. The integer K determines the resolution of the longitudinal discretization and is known in DLCQ as the harmonic resolution [4]. The remaining integrals in Q^- are approximated by a trapezoidal form. The continuum limit in the longitudinal direction is then recovered by taking the limit $K \to \infty$.

In constructing the discrete approximation we drop the longitudinal zero-momentum mode. For some discussion of dynamical and constrained zero modes, see the review [5] and previous work [20,14]. Inclusion of these modes would be ideal, but the techniques required to include them in a numerical calculation have proved to be difficult to develop, particularly because of nonlinearities. For DLCQ calculations that can be compared with exact solutions, the exclusion of zero modes does not affect the massive spectrum [5]. In scalar theories it has been known for some time that constrained zero modes can give rise to dynamical symmetry breaking [5] and work continues on the role of zero modes and near zero modes in these theories [21]. It is possible that a careful treatment of the dynamical zero mode of the gauge field A^+ could give rise to dynamical breaking of supersymmetry of the type suggested in [22].

Our earliest SDLCQ calculations [13] were done using a code written in Mathematica and performed on a PC. This code was rewritten in C++ for the work presented in [14] and has now been substantially revised to reach higher resolutions. We are able to generate the Hamiltonian matrix for $K = 2$ through 7 and for values of T up to $T = 9$ at $K = 4$, decreasing to $T = 3$ at $K = 7$. The actual dimension of the Fock basis as a function of the transverse and longitudinal resolutions is given in Table I. If only one symmetry sector is used, the dimension of the Hamiltonian matrix to be diagonalized is roughly eight times smaller. The absolute limit for the new code, on a Linux workstation with 2GB of RAM, is approximately 32 million states.

We extract several of the lowest eigenstates of the Hamiltonian matrix by applying the Lanczos algorithm [23]. This requires a filtering process to remove spurious states, including copies of the very lowest states, which appear before all the desired states converge.[1] The approach that we take is patterned after the work of Cullum and Willoughby [24]. After n iterations of the Lanczos algorithm, we have an $n \times n$ tridiagonal representation A of the

[1]The appearance of spurious copies is understood [23] as a failure of orthogonality due to accumulation of round-off errors.

TABLE I. The size of the Fock basis as a function of the longitudinal resolution K and transverse cutoff T.

T	$K=4$	5	6	7	8	9
1	150	768	4108	22544	131830	775104
2	522	4142	34834	305016	2753162	25431056
3	1262	13632	156270	1866304	22972270	
4	2498	34160	496106	7505592		
5	4358	72128	1268230			
6	6970	135408				
7	10462	233344				
8	14962	376752				
9	20598	577920				

original Hamiltonian matrix. The spurious eigenvalues of A appear as degenerate copies or are found in the spectrum of the matrix obtained from A by removing the first row and the first column. These two possibilities are easily checked because the tridiagonal matrices are easily diagonalized in full, even though n becomes large, on the order of several thousand. The remaining "good" eigenvalues are checked for convergence, with the number of iterations extended until the desired number or range of converged eigenvalues is obtained. The eigenvectors are readily obtained from the eigenvectors of the tridiagonal matrix A. The only difficulty with the filtering process is the possibility of a "false negative," when a nearly degenerate eigenstate is incorrectly flagged as spurious; we found this type of event to be rare, but, of course, the frequency is dependent on the spectral density and the specific filtering criteria.

In Fig. 1 we show the full spectrum that we obtain as a function of a dimensionless coupling $g' = g\sqrt{NL/4\pi^3}$. This figure shows several striking features that we want to analyze in more detail. First, we observe that the spectrum splits into two bands. At low mass the spectrum is seen as a band of constant height in mass squared for all g'. The upper part of the spectrum appears as a band that grows in width and in mass squared. It is very clear that there is different physics at work in these two bands, and we will analyze them separately. It is also important to note that different numerical methods are required to analyze these sectors. The lowest masses can be found with use of Lanczos diagonalization methods [23]; however, the lowest states in the upper band can only be found from a full diagonalization of the Hamiltonian.

We refer to the lower band in Fig. 1 as the *intermediate-coupling region*, for reasons that will become clear in the next section. We call the upper band the *strong-coupling region*, because these states vary strongly with the coupling. We study them in the strong-coupling limit in Sec. V.

IV. INTERMEDIATE COUPLING

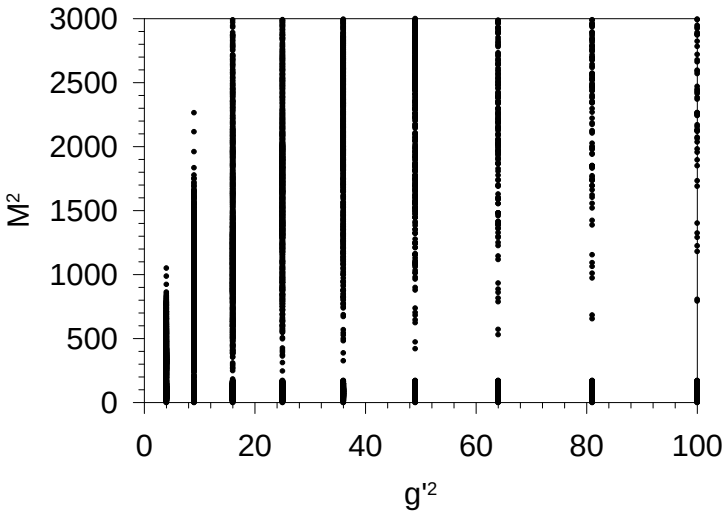

FIG. 1. The full spectrum of M^2 in units of $4\pi^2/L^2$ at resolutions $K = 5$ and $T = 3$ in the $S = +1$, $P = +1$ symmetry sector.

A. Mass spectrum

In Fig. 2 and Fig. 3 we show as functions of g' the average number of partons and the mass squared of bound states in the lower band of Fig. 1. We do this for low and high transverse resolutions. We see that in both cases the average number of particles grows very rapidly with g', and by $g' = 1.5$ the average number is essentially equal to K. The resolution K is the maximum number of partons that are allowed in a state and corresponds to the situation where all the partons have one unit of longitudinal momentum. This should not come as a total surprise, since in the dimensionally reduced version of this model [6,8,9] in 1+1 dimensions we already saw lighter and lighter states with more and more partons appearing as we went to higher resolution. This result suggests that already at intermediate couplings the states are saturating the SDLCQ approximation. That is, we are finding that, at every K, bound states have an average number of particles that is equal to K, the maximum number of particle allowed by the SDLCQ approximation. This implies that the actual states have an average number of particles that is significantly larger than the allowed maximum. Therefore, beyond intermediate values of the coupling, the SDLCQ approximation is missing a significant part of the wave function, and the calculation is becoming unreliable. For this reason we restrict our analysis in this lower band to states with $g' = 0.5$ and 1.0. As we will see below, the dependence of the spectrum on the longitudinal resolution K is stronger than what we have usually seen in SDLCQ, and this is because the approximation is losing significant parts of the wave function at these resolutions.

The other effect that we see in Fig. 2 is a set of states that we previously classified as unphysical [13,14]. Here these states appear at low masses at low transverse resolution, and the mass falls with increasing coupling. We also see in Fig. 2 that there are states with low values of the average number of partons. For these states we find $M^2 \propto \Lambda_\perp^2$, at least approximately. We will find states in the strong-coupling sector that also grow rapidly with transverse resolution as well, and we will return to these unphysical states when we discuss

that sector. In Fig. 3, which shows results at a higher transverse resolutions, the states are no longer visible.

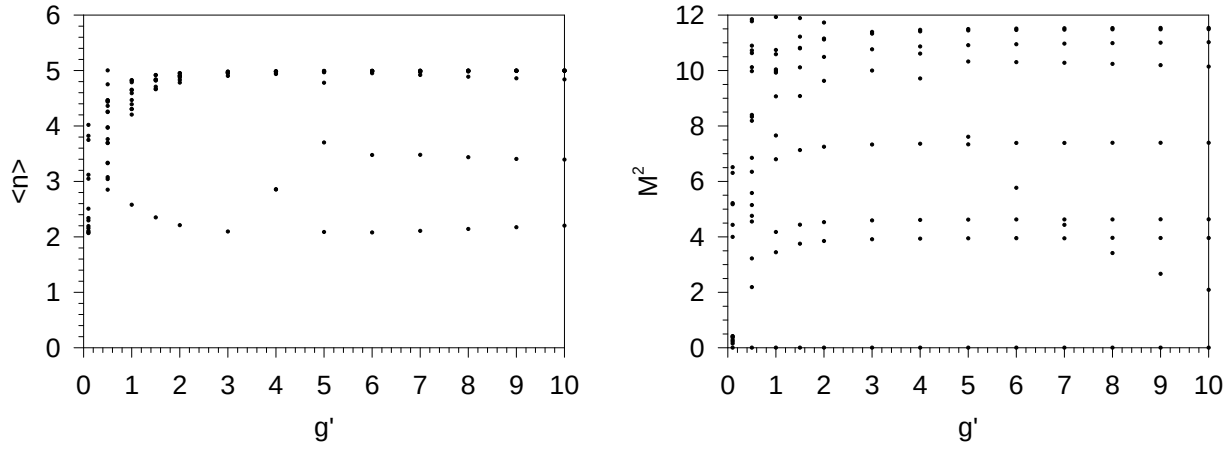

(a) (b)

FIG. 2. Plots of (a) the average number of particles $\langle n \rangle$ and (b) bound-state mass squared M^2 in units of $4\pi^2/L^2$ as functions of the coupling g' at resolutions $K = 5$ and $T = 2$ in the $S = +1$, $P = -$ symmetry sector.

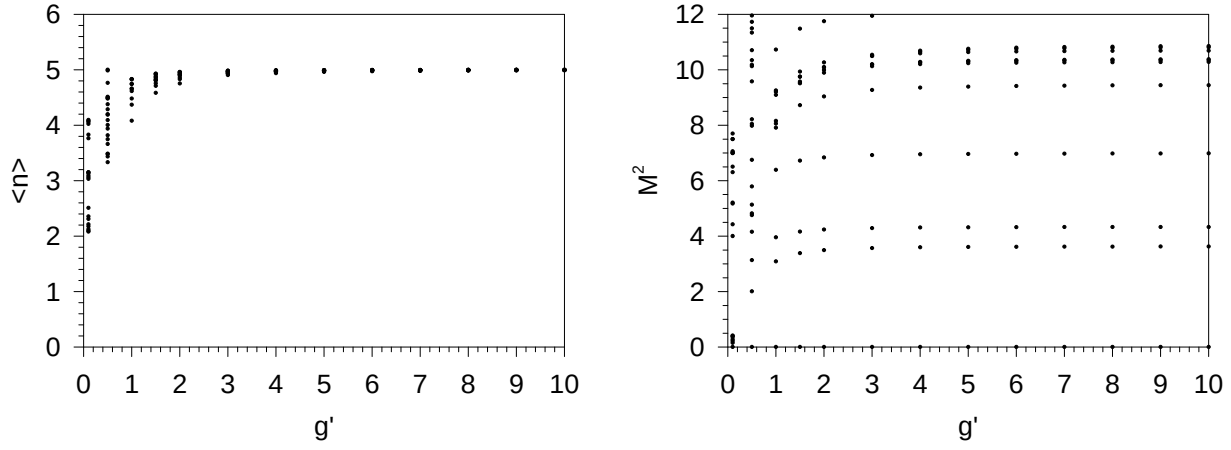

(a) (b)

FIG. 3. Same as Fig. 2 but for $T = 9$.

A detailed analysis of a few intermediate-coupling bound states will be done in two steps. At fixed longitudinal resolution K, we will identify a sequence of states at different values of the longitudinal resolution T that correspond to the same bound state. We make this identification using the properties of the state, most notably the mass, the average number of fermions, and the average momentum of the fermions. We have calculated a large number of other average properties of the bound states, but they are less useful in distinguishing states. We then plot this set of states as a function of $1/T$ and make a linear fit. The intercept is the mass at a particular value of K with an infinite transverse-momentum cutoff. We then

plot these cutoff-independent masses as a function of $1/K$ and make a second linear fit. The intercept is the mass at infinite longitudinal resolution. By this method we identify the mass that is independent of the transverse momentum cutoff and of the longitudinal resolution. These bound states are at a fixed value of the coupling, and the mass scale is set by the transverse length scale.

As we discussed earlier, this theory has two exact symmetries, parity P and S symmetry, and the problem of calculating the spectrum is divided into 4 sectors, $P = \pm 1$ and $S = \pm 1$. The P symmetry gives rise to a doubling of the spectrum; this degeneracy is in addition to the fermion-boson degeneracy. These P-degenerate pairs are in fact not simply related. For example, in one sector a state may have an average number of fermions $\langle n_F \rangle$ equal to 2, while in the other sector it might have $\langle n_F \rangle = 0$. This property proves to be very useful in identifying sequences of bound states at different K and T. While two states might appear very similar in one P sector, they can be very different in the other sector.

The two S sectors give rise to different sets of bound states, one for $S = +1$ and another for $S = -1$. For each bound-state mass there will be two states with different properties, one corresponding to $P = +1$ and one corresponding to $P = -1$. We will present here the four lowest states in each S sector. We label these states as $2.5\pm$, $3.0\pm$, $3.5\pm$ and $4.0\pm$ for convenience.

As we mentioned earlier, in this theory the average number of particles in a bound state grows as the mass of the bound state decreases. Therefore, the lightest massive bound state has a large number of particles. The maximum number of particles allowed by the approximation is the resolution, K. At $K = 7$ and $K = 6$ we are only able to include T up to 3 and 5, respectively. The two lowest mass states in each sector are only seen for $K = 6$ or 7, and for these cases we do not attempt to make a linear fit in $1/K$ but rather we just use the average T intercept for the mass. The $1/T$ curves for these states, $2.5\pm$ and $3.0\pm$, are shown in Fig. 4 for $g' = 0.5$ and 1.0, and the properties are given in Table II.

Finally, we have states that can be identified at three values of K and other states that can be identified at four values of K. In Fig. 5 we show these states for the sector $S = +1$ and coupling $g' = 1.0$, while in Fig. 6 we show the lowest states at coupling $g' = 0.5$. Similarly in Fig. 7 and 8 we show the lowest states in the $S = -1$ sector with $g' = 1.0$ and $g' = 0.5$, respectively. The properties of each are given in Table III.

TABLE II. Masses M^2 and average fermion number $\langle n_F \rangle$ for the states in Fig. 4. The masses are in units of $4\pi^2/L^2$.

M^2	1.52	2.30	2.39	3.10	1.78	1.96	2.73	2.85
g'	0.5	0.5	1.0	1.0	0.5	0.5	1.0	1.0
S	+	+	+	+	-	-	-	-
$\langle n_F \rangle$ with $P = +1$	2	0.5	2	0	2	2	2	2
$\langle n_F \rangle$ with $P = -1$	2	2[a]	2[a]	2[a]	2	0	2	0

[a]These assignments are based on the symmetry pattern observed in Table III, *i.e.*, low-mass, $S+$, $P-$ states appear to have two fermions.

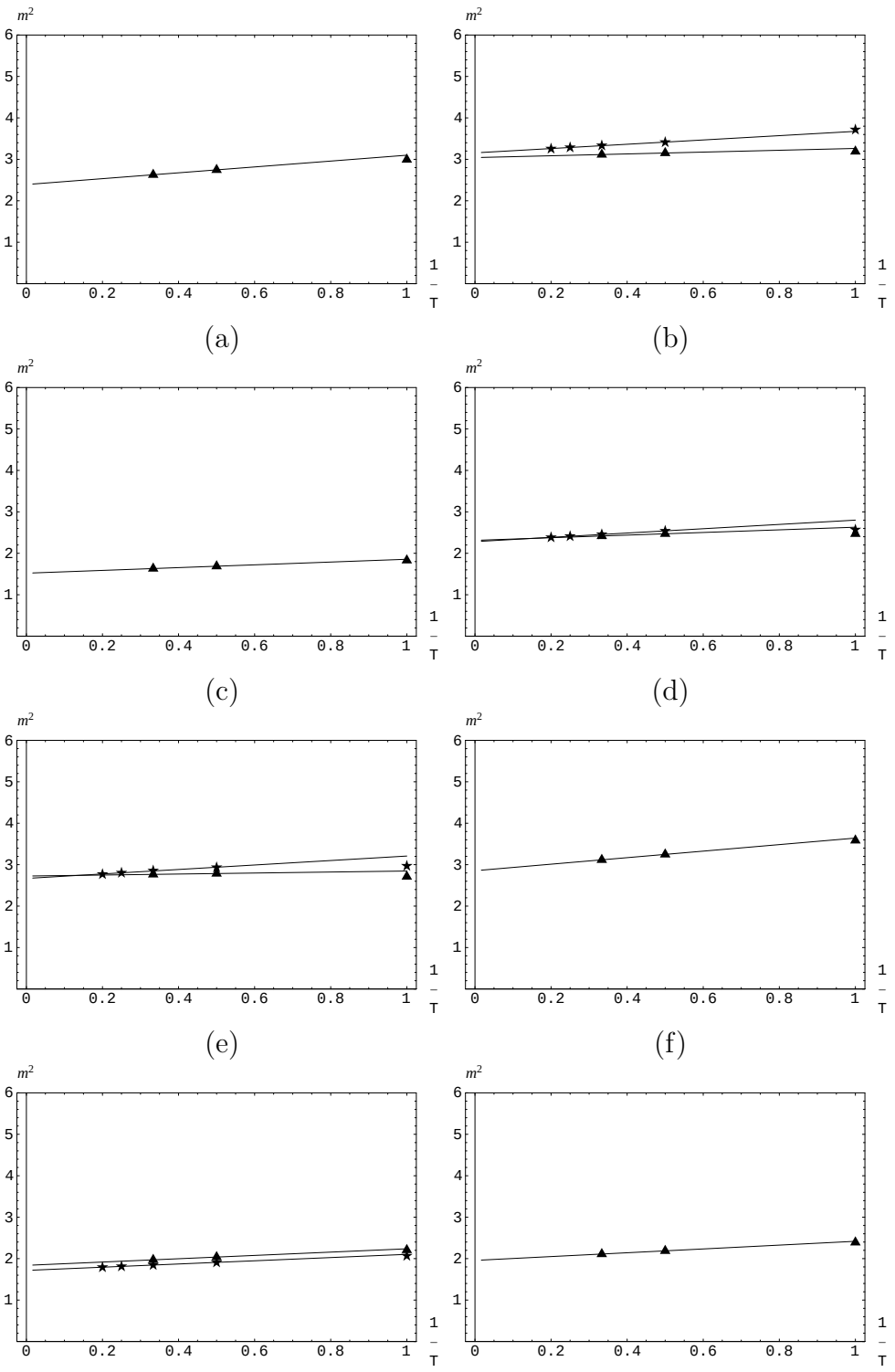

FIG. 4. Bound-state masses squared M^2 in units of $4\pi^2/L^2$ as functions of $1/T$ for (a) states 2.5+, $g' = 1.0$; (b) states 3.0+, $g' = 1.0$; (c) states 2.5+, $g' = 0.5$; (d) states 3.0+, $g' = 0.5$; (e) states 2.5−, $g' = 1.0$; (f) states 3.0−, $g' = 1.0$; (g) states 2.5−, $g' = 0.5$; (h) states 3.0−, $g' = 0.5$. The longitudinal resolutions are $K = 6$ (stars) and 7 (triangles).

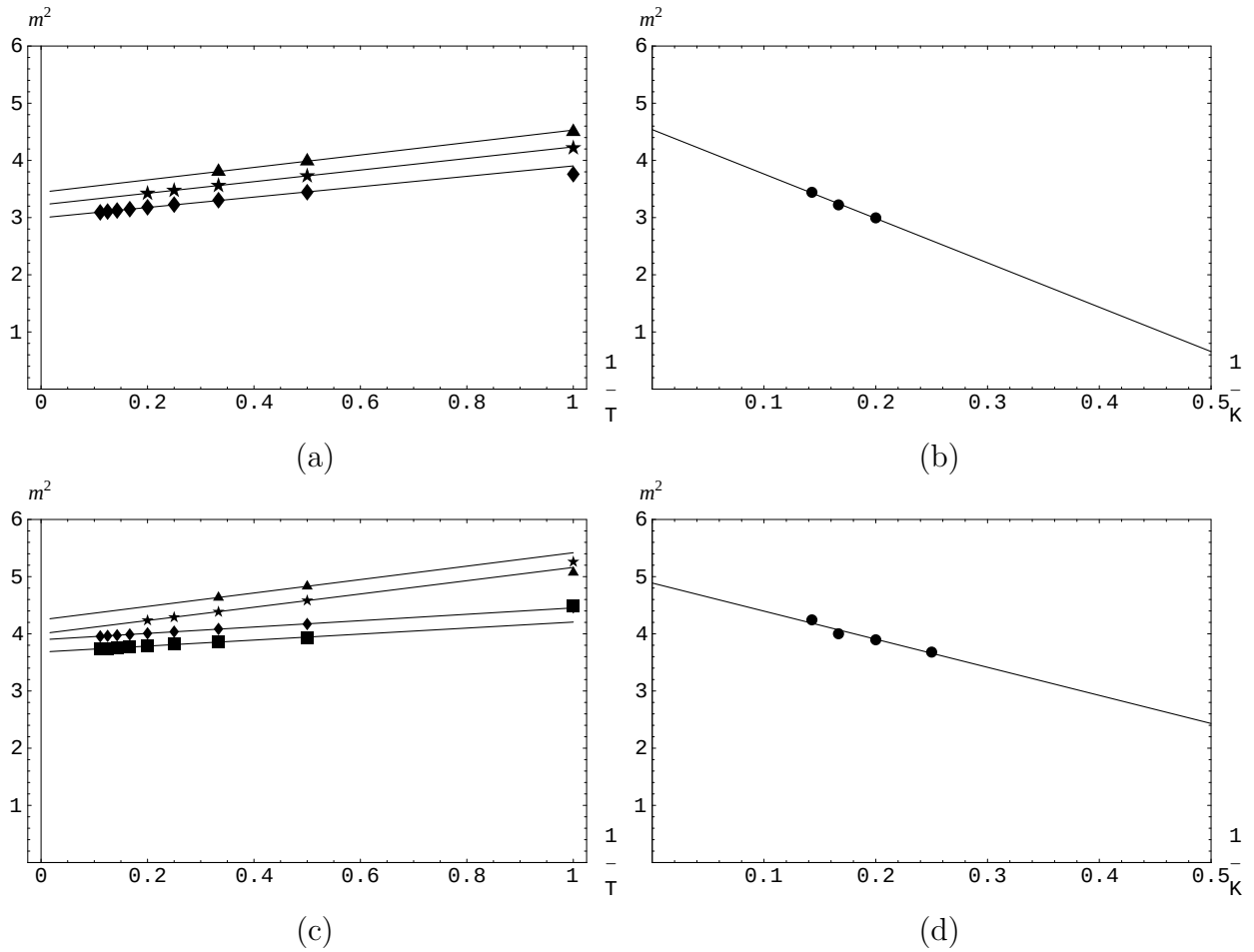

FIG. 5. Bound-state masses squared M^2 for the $S = +1$ sector in units of $4\pi^2/L^2$ at coupling $g' = 1.0$ for (a) the state 3.5 as a function of $1/T$ for different values of K and fit to straight lines, (b) intercepts from (a) plotted as a function of $1/K$, (c) the state 4.0 as a function of $1/T$ for different values of K and fit to straight lines, and (d) intercepts from (c) plotted as a function of $1/K$. The longitudinal resolutions are $K = 4$ (squares), 5 (diamonds), 6 (stars), and 7 (triangles).

B. Structure functions

So far, we have only discussed the integrated properties of the wave functions of the individual states. It is, however, very instructive to look at the structure functions. The fact that we saw very good convergence will be reflected in the invariance of the shape of the structure function of a given bound state seen at different T and K.

We use a standard definition of the structure functions

$$\hat{g}_A(x,k^\perp) = \sum_q \int_0^1 dx_1 \cdots dx_q \int_{-\infty}^{\infty} dk_1^\perp \cdots dk_q^\perp \delta\left(\sum_{i=1}^q x_i - 1\right) \delta\left(\sum_{j=1}^q k_j^\perp\right) \times \sum_{l=1}^q \delta(x_l - x)\delta(k_l^\perp - k^\perp)\delta_{A_l}^A |\psi(x_1,k_1^\perp;\ldots x_q,k_q^\perp)|^2 . \quad (4.1)$$

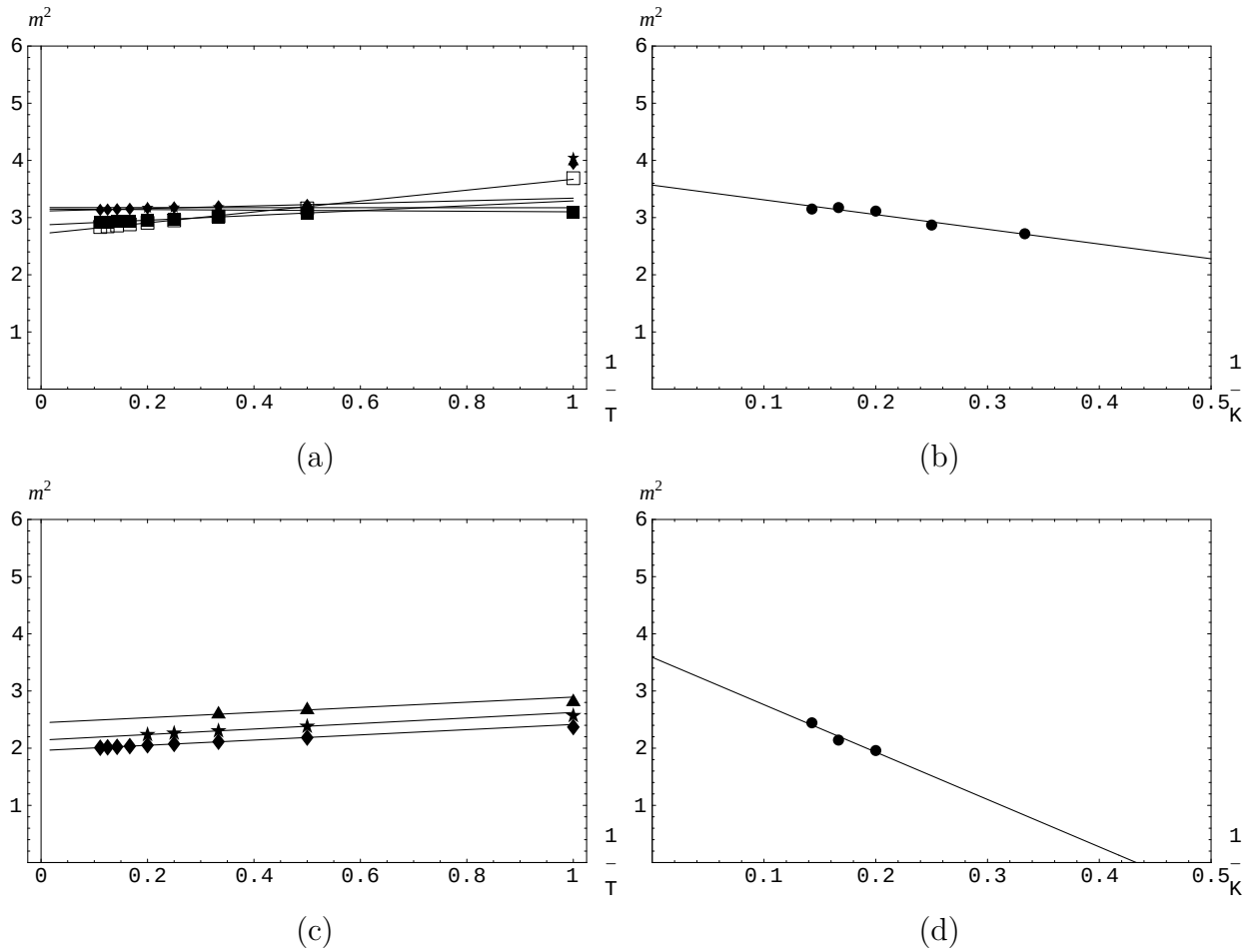

FIG. 6. Same as Fig. 5 but for $g' = 0.5$. The open squares represent longitudinal resolution $K = 3$.

Here A stands for either a boson or a fermion. The sum runs over all parton numbers q, and the Kronecker delta $\delta^A_{A_l}$ selects partons with matching statistics A_l. The discrete approximation g_A to the structure function $\hat{g}_A$, with resolutions K and T in longitudinal and transverse momentum, is

$$g_A(n, n^\perp) = \sum_{q=2}^{K} \sum_{n_1,\ldots,n_q=1}^{K-q} \sum_{n_1^\perp,\ldots,n_q^\perp=-T}^{T} \delta\left(\sum_{i=1}^{q} n_i - K\right) \delta\left(\sum_{j=1}^{q} n_j^\perp\right) \times \sum_{l=1}^{q} \delta_n^{n_l} \delta_{n^\perp}^{n_l^\perp} \delta^A_{A_l} |\psi(n_1, n_1^\perp; \ldots n_q, n_q^\perp)|^2 \,. \tag{4.2}$$

The functions $g_A(n, n^\perp)$ are normalized so that summation over both arguments gives the average boson or fermion number; their sum is then the average parton number, and we compute these sums as a test.

We focus on the state in the $S = -1$ sector which has a continuum mass of $M^2 = 3.52$. This state will have different manifestations at different cutoffs K and T, and we have to ask the following questions. Firstly, are the structure functions stable enough against variations in both cutoffs to identify states at different K and T, and, secondly, are they distinct

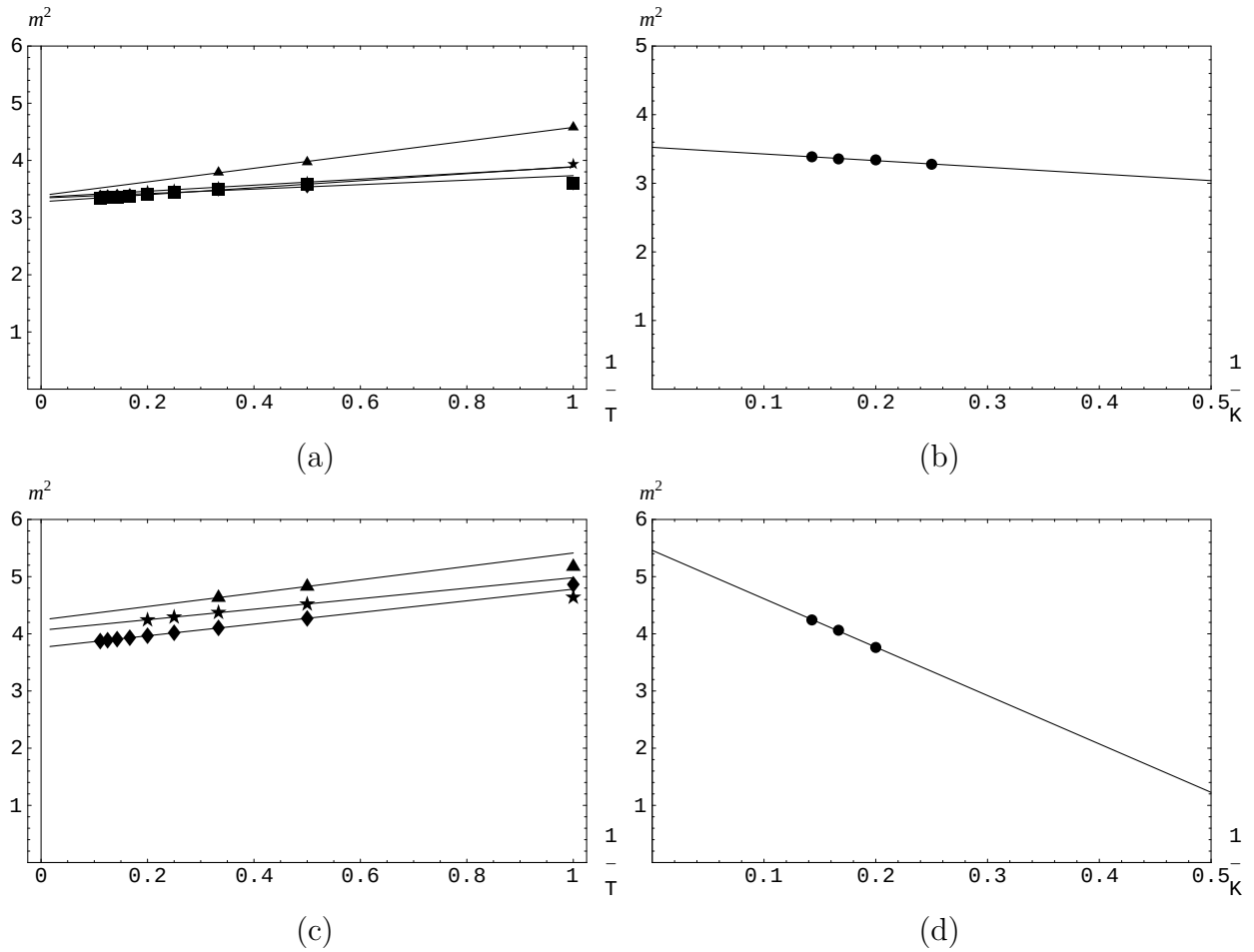

FIG. 7. Same as Fig. 5 but for the $S-$ sector.

enough for different states, so that we can distinguish between states that are close in mass and other integrated properties of their wave function?

To address the first question, consider Fig. 9, where we present plots of the boson and fermion structure functions of the state. It is important to keep in mind that in each plot there are *four* curves, corresponding to different transverse cutoff values and to different amounts of longitudinal momentum. The curves with the higher amplitude in each plot are the probability to find the parton with a longitudinal momentum of $n = 1$, and the low-amplitude curves are the probability to find the same parton with $n = 2$. We suppress curves with $n \geq 2$, because of their much smaller amplitudes.

The first thing to notice is that the shapes of all states are nearly invariant under a change of the transverse cutoff T. Unfortunately, this means that the (dashed and solid) lines are almost indistinguishable. The only thing that changes is the actual cutoff in $n^{\perp}$: the curves have support only up to a maximum $n^{\perp}_{\rm max} = T$. This might be also hard to see in the plots, and we put vertical lines in each plot at the points $n^{\perp} = \pm 3$, where the support of the structure function at the smaller transverse cutoff ends. This behavior is contrary to the one in the longitudinal direction, where a larger K is synonymous with a better resolution of the wave function. Here, however, a change of T clearly is a change of the cutoff $\Lambda_{\perp} = 2\pi T/L$, where L is the fixed transverse box size.

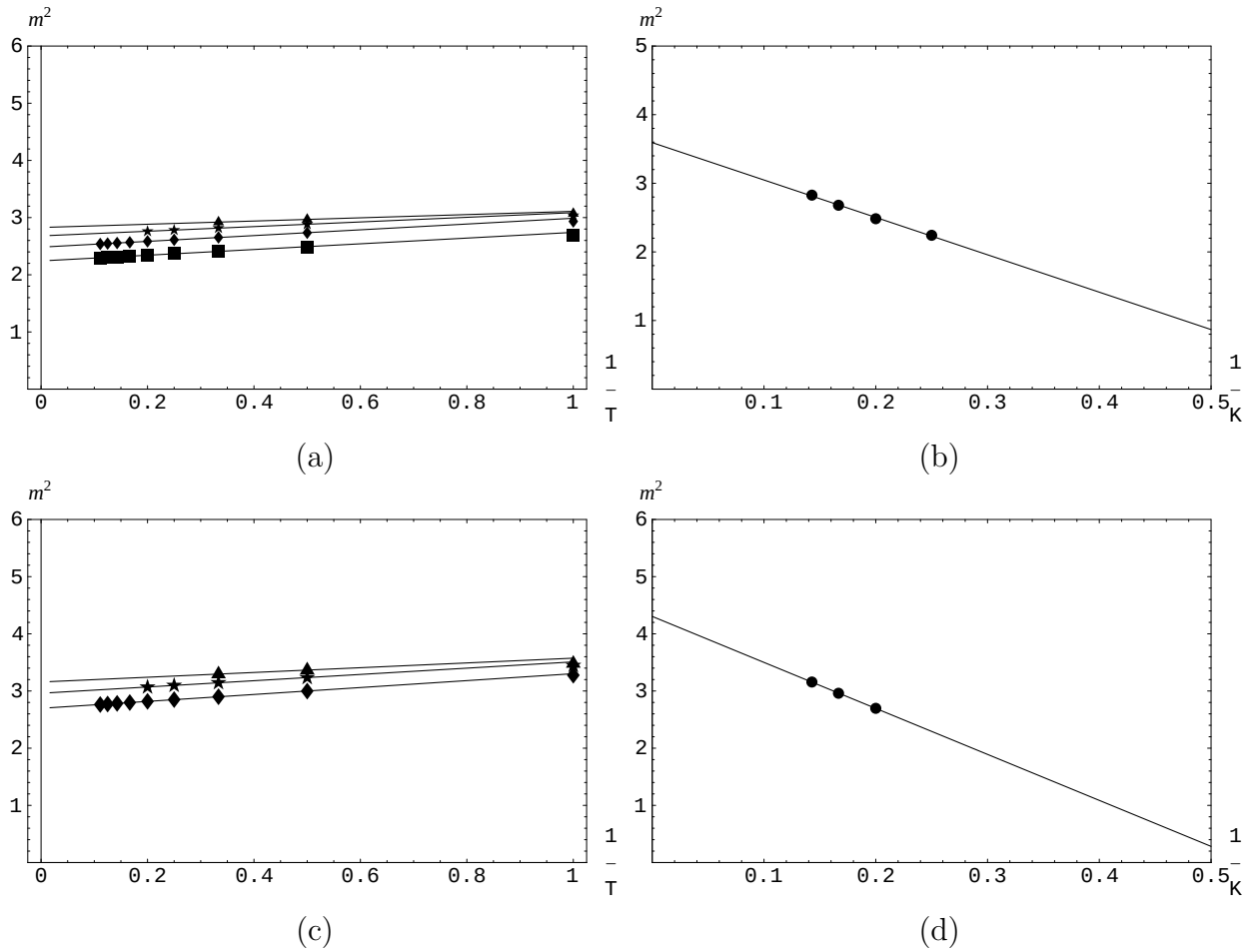

FIG. 8. Same as Fig. 6 but for the $S-$ sector.

Having established this remarkable stability in T, let us now look at how the structure function changes as K grows. In Fig. 9 we have to compare the functions in the two upper plots. We see that they are very close in shape, although the peak values change. A discussion of the differences in peak value is in order. In Fig. 9, we see that the peak values are the same for the fermion structure functions at different K, but are different for the boson structure functions. The reason for this becomes clear if we look at the properties of this state: the average fermion number stays constant with K, whereas the average parton number grows considerably. The latter fact is what we see in Figs. 2 and 3, and it also tells us that we mainly add partons with vanishing $n_\perp$, as we go higher in K. A quick look at the fermion structure functions in the lower row of Fig. 9 reveals a consistent behavior. Again, we see no dependence on the transverse cutoff T. The curves are a perfect match at different K.

Now that the shape invariance of the structure functions has been extended to changes in both K and T, let us address the second question, of whether the structure functions are different enough to distinguish states. Consider Fig. 10, where the state with continuum mass squared $M^2 = 3.52$ is plotted (*cf.* Fig. 9) at $T = 5$ for $K = 5$ and $K = 6$, together with the next lightest state with $\langle n_F \rangle = 2$ in both parity sectors at $K = 6$, which has a mass $M^2 = 2.73$ according to Table II. It is immediately clear that the latter state is different

TABLE III. Masses M^2 and average fermion number $\langle n_F \rangle$ for the states in Figs. 5, 6, 7, and 8. The masses are in units of $4\pi^2/L^2$.

M^2	3.57	3.59	4.54	4.89	3.59	4.30	3.52	5.46
g'	0.5	0.5	1.0	1.0	0.5	0.5	1.0	1.0
S	+	+	+	+	−	−	−	−
$\langle n_F \rangle$ with $P = +1$	0	2	2	0	2	2	2	2
$\langle n_F \rangle$ with $P = -1$	2	2	2	2	2	0	2	0

and cannot be a manifestation of the one with $M^2 = 3.52$: both the $n = 1$ and the $n = 2$ components of the structure function have different shapes, even if we would scale them to have the same peak values. The shape of the structure function of a state seems, therefore, a very characteristic and stable property of each individual state.

V. STRONG COUPLING

Our analysis of the strong-coupling region (the upper band of Fig. 1) can only be considered preliminary at this stage, since these states are in the middle of the spectrum and one therefore needs a full diagonalization of the Hamiltonian to reach them. This severely limits the values of K and T that we can consider. Nevertheless, we think it is worth taking a look at this part of the spectrum.

The Hamiltonian matrix is a quadratic matrix polynomial in g', and, therefore, it is natural to consider M^2/g'^2 as a function of $1/g'^2$. In Fig. 11 we show plots for $K = 5$ and $T = 1$, 2 and 3. At the bottom of the strong-coupling band, several clear sets of separate masses appear. They seem to move linearly as functions of $1/g'^2$, and it is natural to identify them as bound states. From these three figures it is clear that these states have a strong T dependence. In Fig. 11(d) we plot the intercept of a linear fit in $1/g'^2$ to the lowest state in the strong-coupling band. While we only have three points, they clearly appear to have linear behavior in T.

In fact, if we look at the full spectrum as a function T, as shown in Fig. 12, we see that the entire strong-coupling band appears to grow linearly with T, as the state we just discussed behaves. Given this behavior in T, it is not clear whether we should take these states seriously. If we view these states in terms of dimensionful quantities, the gauge coupling g_{YM} and the transverse cutoff $\Lambda_\perp = 2\pi T/L$, we see that the physical mass squared $\mathcal{M}^2$ is proportional to $g_{YM}^2 N_c \Lambda_\perp$. This is an expression for the bound-state mass that is independent of the length scale L; it is, however, not what one expects for the continuum limit for the bound states of a finite theory with only one dimensionful parameter, g_{YM}. As we commented in [14], one would expect the continuum mass of such a theory to behave like $(g_{YM}^2 N)^2$.

We know that this is a totally finite theory, so it would appear that this behavior is very strange. It is interesting to look at the structure functions for some of these states. In Fig. 13(a) we show the structure function of the lowest state in the strong-coupling band for various values of T. Around zero transverse momentum we see in this figure a bound state similar to the bound states we saw in earlier structure functions. This central peak

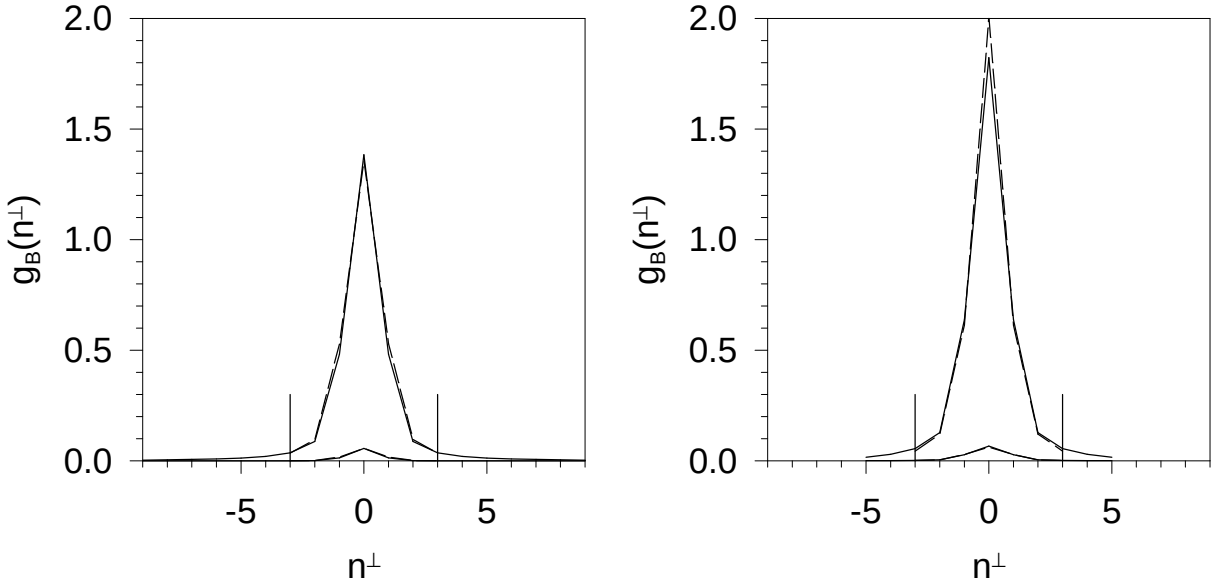

(a) (b)

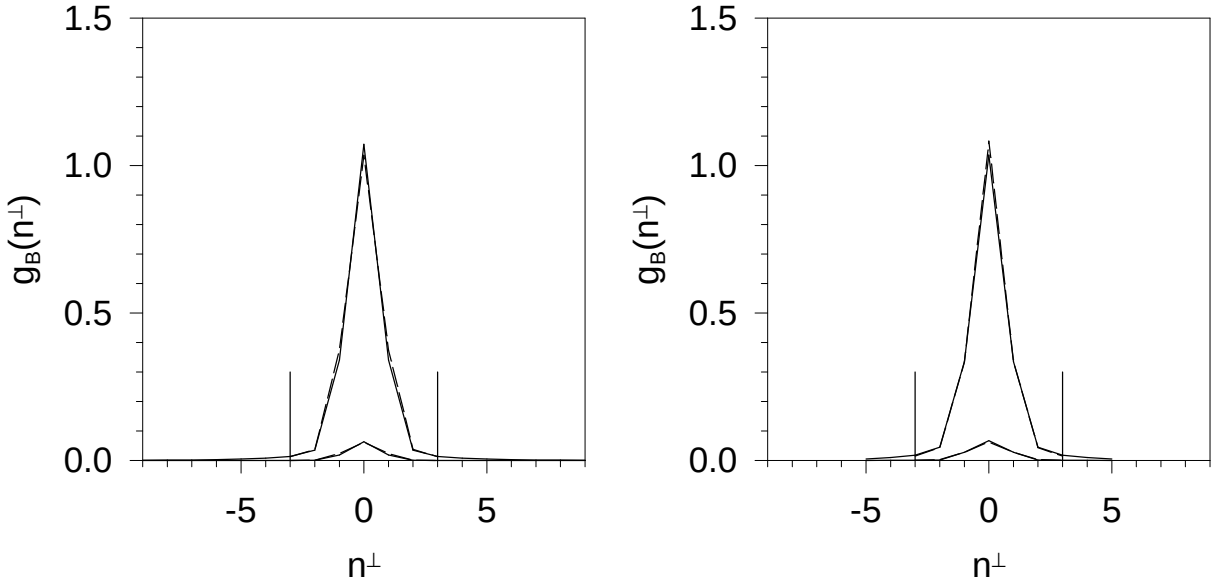

(c) (d)

FIG. 9. Structure functions for the bound state with mass $M^2 = 3.52$ at different K and T. Top row: boson structure functions. Left (a): $K = 5$ at $T = 3$ (dashed line) and $T = 9$ (solid line). Right (b): $K = 6$ at $T = 3$ (dashed line) and $T = 5$ (solid line). Bottom row: fermion structure functions. Left (c): $K = 5$ at $T = 3$ (dashed line) and $T = 9$ (solid line). Right (d): $K = 6$ at $T = 3$ (dashed line) and $T = 5$ (solid line). The vertical lines mark the range in $n^\perp$ for T=3.

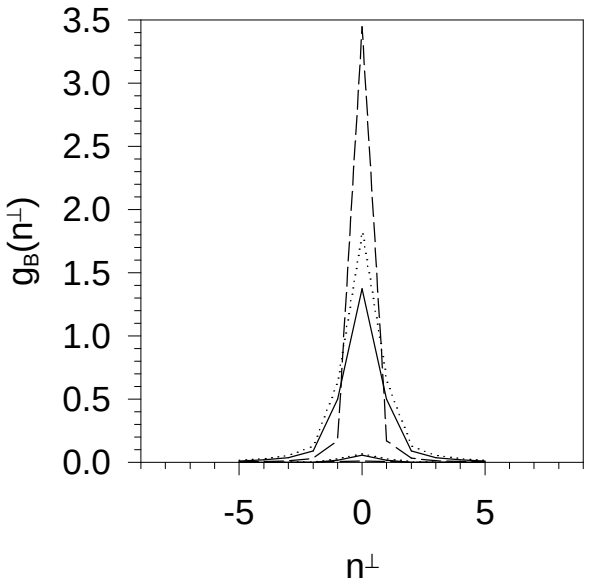

FIG. 10. Structure functions of two manifestations of the same state at different $K = 5, 6$ and a distinct state at $K = 6$: the state with continuum mass $M^2 = 3.52$ for $K = 5$ (solid line) and $K = 6$ (dotted line); the state with continuum mass $M^2 = 2.73$ for $K = 6$ (dashed line). For all cases the value of T is 5, the symmetry sector is $S = -1$, $P = +1$, and the coupling is $g' = 1$.

converges quickly in T and cannot be the main reason for the T dependence of this state. It rather comes from the wings that appear at large transverse momentum. As we increase T, we see a larger and larger part of these bound states, and this gives rise to the strong T dependence of the total state.

In Fig. 13(b) we show the structure functions of two other states in the strong-coupling band. These states do not have the central peak as the one in Fig. 13(a), and the large wings that we saw before are replaced by two bumps at non-zero momentum. It appears that the property that characterizes these states in the strong-coupling band is this multi-hump distribution function.

We now return to the unphysical states that we saw in the intermediate-coupling band. It is convenient to consider them at large coupling even though they are in the intermediate coupling band. The identifying property of these states is their low average parton number. When $K = 4$ and $g' = 10$, most states have $\langle n \rangle \simeq 4$, whereas these states have $\langle n \rangle \simeq 2$. The mass of the lowest of these states grows rapidly with T, similar to the states that we found in the strong-coupling band.

The structure function for this state is shown in Fig. 14. We see a shape that is somewhat similar to those for states in the strong-coupling band. There now appear to be three bound states with all three peaks resolved but not cleanly separated. We see that, as the transverse resolution is increased from three to nine, the three peaks become much more distinct. There is no doubt that this change gives rise to the strong T dependence. It is not clear at this time exactly why certain of these multi-hump distributions appear in the lower band and others appear in the upper band.

Let us now turn to some of the global properties of the full spectrum. In Fig. 15 we show

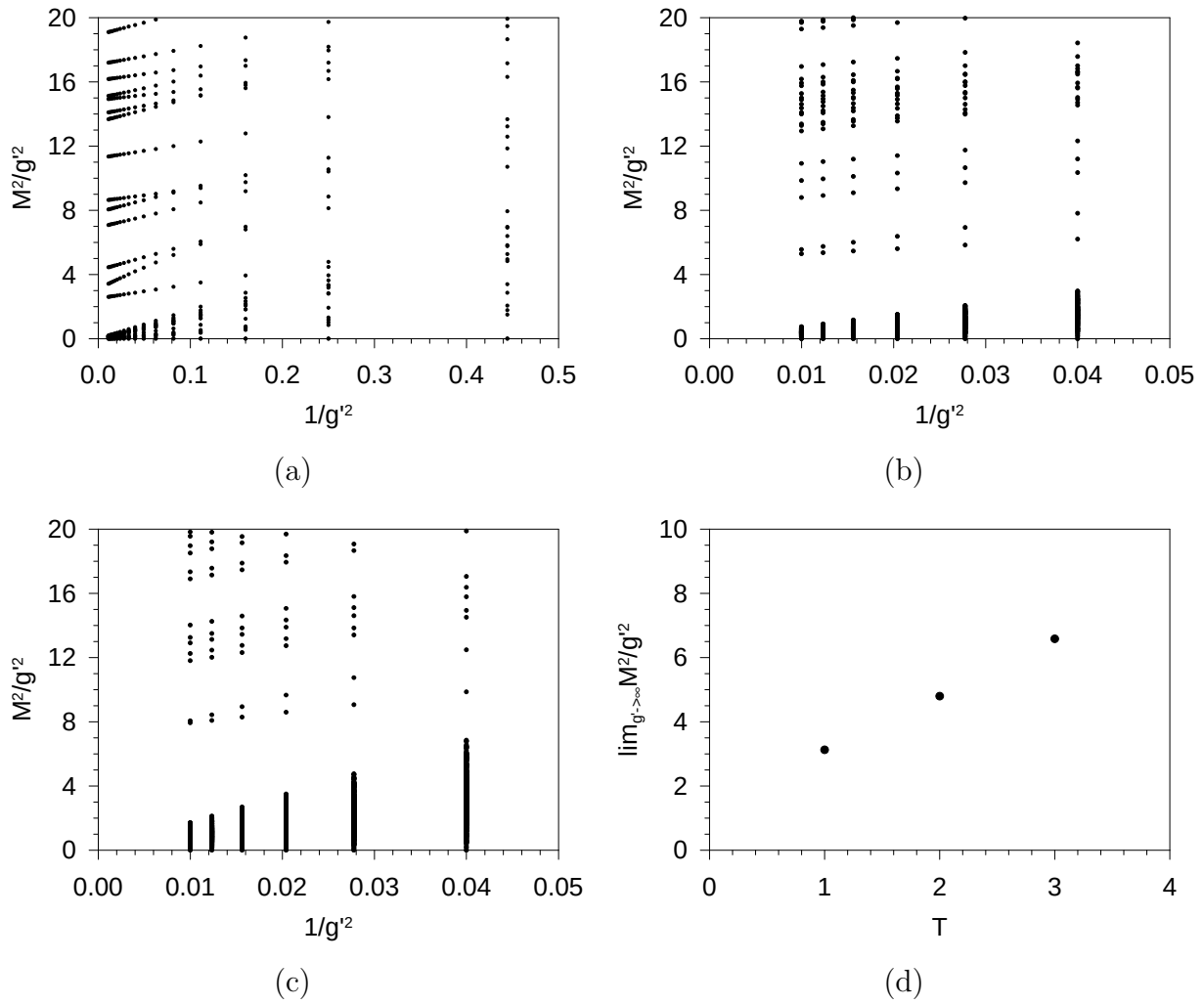

FIG. 11. Bound-state masses squared M^2 in units of $4\pi^2/L^2$ divided by g'^2 as functions of $1/g'^2$ in the symmetry sector $S = +1$, $P = +1$ for $K = 5$ and (a) $T = 1$, (b) $T = 2$, and (c) $T = 3$; and (d) the T dependence of the intercepts of the lowest-mass state in the strong-coupling sector of (a), (b), and (c).

the bound-state spectrum as a function of the average number of particles at $K = 5$, $T = 1$ and $K = 6$, $T = 1$. We superimpose the spectra for $g' = 0.1$, 0.5, 1, 1.5, 2, 3, 4,...,10. As we noted previously, the density clusters near the maximum value allowed for $\langle n \rangle$, which is K. In addition we see sets of trajectories with increasing masses at small $\langle n \rangle$. In fact, these trajectories with the low $\langle n \rangle$ correspond to the most massive states in the entire spectrum.

In Fig. 16 we show the bound-state spectrum as a function of the average number of fermions. In spite of the fact that we are dealing with a supersymmetric theory, the average number of fermions behaves quite differently than that of the bosons. It does not appear to grow nearly as fast. In the intermediate-coupling region we saw that the number of fermions was nearly a sharp quantum number in the bound state, that is $\langle n_F^2 \rangle = \langle n_F \rangle^2$. In comparing the figures for $K = 5$ and $K = 6$, in Fig. 16, we see a particularly striking feature: there are no states in the range from 4 to 6 for $K = 6$. That is, all the bound states with six fermions

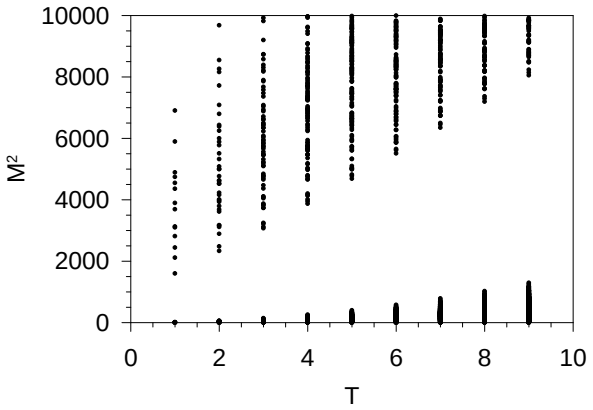

FIG. 12. Bound-state masses squared M^2 in units of $4\pi^2/L^2$ as functions of T, for the symmetry sector $S = +1$, $P = +1$, longitudinal resolution $K = 4$, and coupling $g' = 10$.

have exactly six fermions. The interpretation of this fact is not yet clear.

VI. DISCUSSION

In this paper we present a first-principles calculation of the massive spectrum and the wave functions of $\mathcal{N} = 1$ SYM theory in 2+1 dimensions. This is the first such calculation and will provide a benchmark for future calculations using lattice and other methods. The calculation was performed using SDLCQ, which has been successfully applied to a number of (1+1)-dimensional theories. The success of this method stems from its retention of supersymmetry at every step of the numerical approximation.

In our formulation this theory has three exact symmetries: supersymmetry, parity P, and an orientation symmetry we call S. These are all Z_2 symmetries, and they allow us to reduce the size of the matrices in the numerical approximation by a factor of 8. Supersymmetry and parity give rise to a four-fold degeneracy which is now split between different symmetry sectors. The elimination of this four-fold degeneracy simplifies the application of the Lanczos diagonalization algorithm.

The theory has three dimensionful constants with the dimension of (length)$^{-1}$: $g_{YM}^2 N_c$; $\Lambda_\perp$, the transverse momentum cutoff; and $1/L$, the reciprocal of the length of the compact dimension. We find spectra that behave as $1/L^2$, $g_{YM}^2 N_c \Lambda_\perp$, and $\Lambda_\perp^2$. In Fig. 1 we see that the spectrum divides into three regions, a weak-coupling region and two bands at higher coupling. The weak-coupling region is discussed in detail in Ref. [14]. There we found massless states and very light states that are totally determined by the (1+1)-dimensional theory, as well as heavier states whose masses come primarily from the transverse momentum of the constituents. These states all scale like $1/L^2$.

Of the two bands at higher coupling, we call the lower one the intermediate-coupling band. Most of the bound states in this band are dominated by a very large number of constituents as the coupling gets strong. This fact limits the region in coupling space that we can explore using SDLCQ. We have explored this region up to an intermediate coupling, and we find a well defined spectrum which converges very rapidly as we increase the transverse

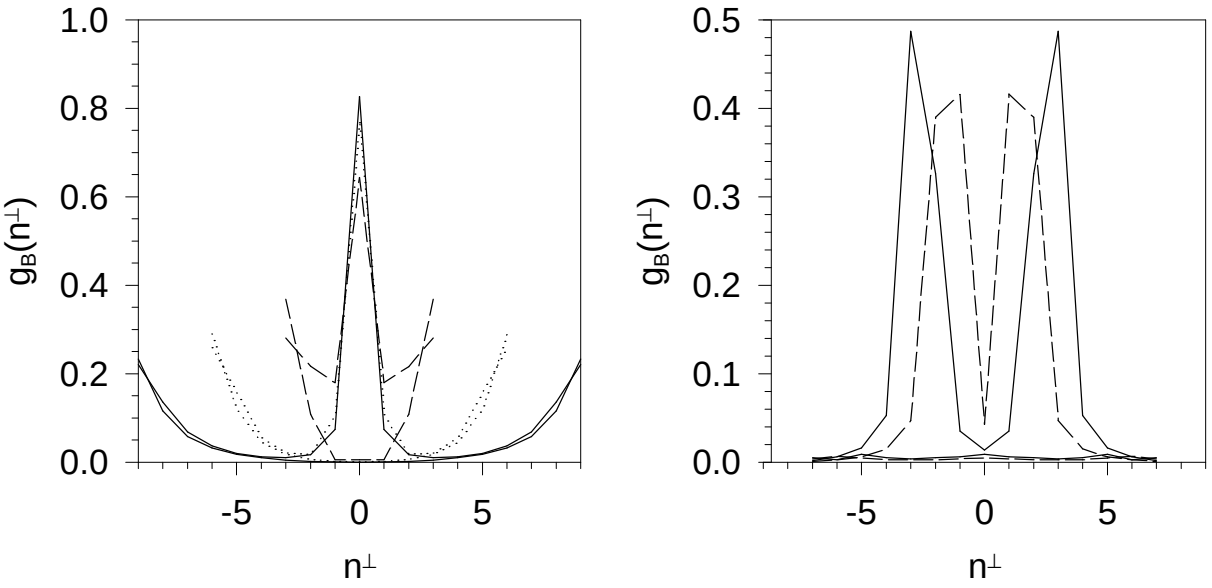

(a) (b)

FIG. 13. Structure functions for some massive states in the strong-coupling sector: (a) the lowest state in the sector, at $T = 3, 6, 9$ (dashed, dotted, solid lines, respectively), and (b) two very massive states with $M^2 = 24,625$ (dashed line) and $M^2 = 22,728$ (solid line). For all cases, the symmetry sector is $S = +1$, $P = +1$, the longitudinal resolution is $K = 4$, and the coupling is $g' = 10$.

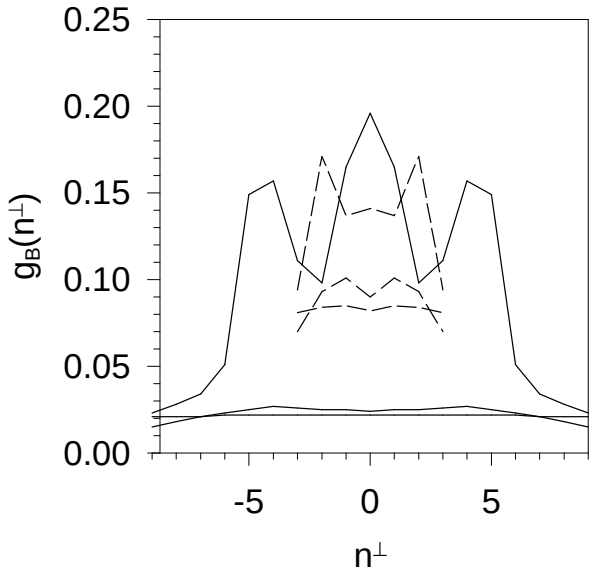

FIG. 14. Structure functions for an unphysical state. Shown are the probabilities to find a boson with longitudinal momentum $n = 1, 2, 3$ (each with decreasing amplitude) for different cutoffs $T = 3$ (dashed lines) and $T = 9$ (solid lines). The symmetry sector is $S = +1$, $P = +1$, the longitudinal resolution is $K = 4$, and the coupling is $g' = 10$.

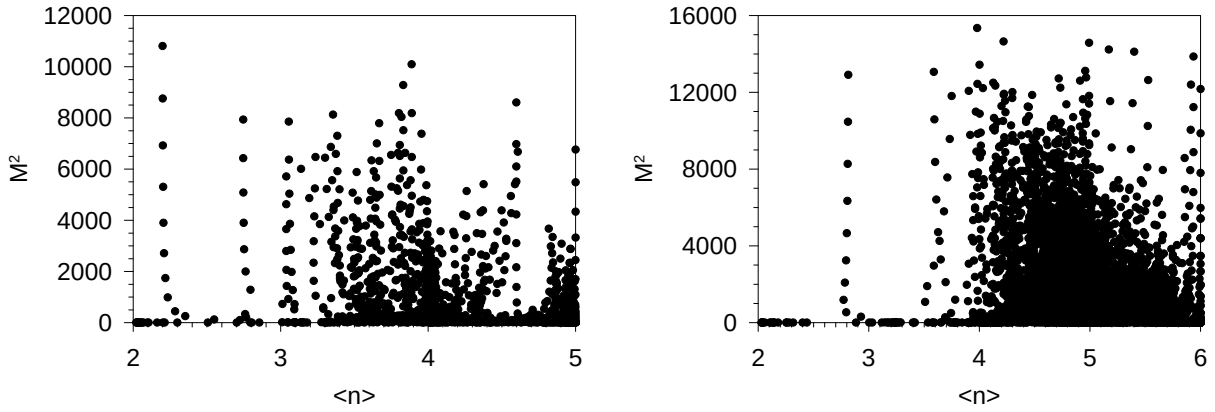

(a) (b)

FIG. 15. Bound-state masses squared M^2 in units of $4\pi^2/L^2$ as functions of the average number of particles $\langle n \rangle$ for (a) $K = 5$, $T = 1$ and (b) $K = 6$, $T = 1$. Several different values of the coupling are included; they are $g' = 0.1$, 0.5, 1, 1.5, 2, 3, 4,...,10. The symmetry sector is $S = +1$, $P = +1$.

momentum cutoff. We also found that the transverse momentum distributions converge exceptionally well with transverse momentum cutoff. Convergence in the longitudinal resolution is not as rapid as the transverse convergence, but it still appears to be well behaved. We extrapolate to infinite resolution in both the longitudinal and transverse directions and present a list of some of these states and their properties. The masses of all of these states scale like $1/L^2$. It is interesting to note that, while the average number of particles grows rapidly with the coupling, this is not true for the average number of fermions. Typically the states we studied in this band have precisely either zero fermions or two fermions. In fact, this is a property that persists throughout the full spectrum. It is as if each bound state has a valence number of adjoint fermions that characterizes the state.

In addition to these states, there are other states in the intermediate-coupling band that we discussed previously [13,14] and have called unphysical states. The distinctive properties of these states are that the average number of particles is small and does not appear to saturate the resolution. The transverse momentum distributions are multi-humped, and the masses grow like $\Lambda_\perp^2$ and fall with increasing coupling. Therefore, as we take the transverse cutoff to infinity, these states appear to decouple. It could be of some importance to find a physical meaning for these states, because they have a small average number of particles, as one might expect in a QCD-like theory, but even if their masses were to stabilize at some large transverse cutoff beyond what we currently can reach, they would be so massive that it is hard to see how they could be relevant. The only hope might be that at some very large coupling they fall back into an interesting region.

In the strong-coupling band we found states that scaled like $g_{YM}^2 N_c$ at large coupling. We were motivated to look for this behavior because the supercharge is linear in the coupling. These states have multi-hump transverse momentum distributions, and their masses go like $g_{YM}^2 N_c \Lambda_\perp$. We saw that some of the transverse momentum distributions have two clearly separated and symmetric humps. It is as if half of the constituents in these bound states are going one way while the other half are going the other way, leaving no constituents that are

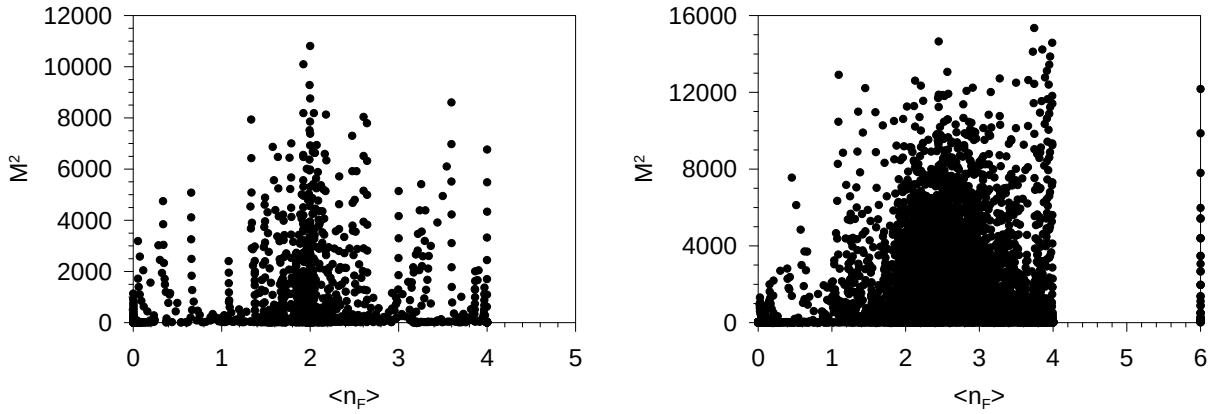

(a) (b)

FIG. 16. Same as Fig. 15 but for masses as functions of the average number of fermions $\langle n_F \rangle$.

at rest relative to the center of mass of the bound state. It almost appears as though we are looking at two bound states [25,26]. If this were the case we would expect to see the same bound states elsewhere in the spectrum with a different relative transverse momentum and a different total energy. We have looked for these states but could not find them. Also, this picture does not naturally seem to lead to an explanation of the linear growth of the mass with the transverse momentum cutoff.

We have looked at the global properties of this strongly coupled band and found unusual behavior as a function of the average number of fermions and of the average number of particles. Numerical limitations unfortunately make this band more difficult to investigate, and, while it remains possible that interesting physics might emerge from these states, the most likely result is that they decouple from the physical spectrum. We must note that we do not find states that scale as $g_{YM}^4 N_c^2$, which is the dependence one would expect in R^3, where the coupling is the only dimensionful parameter in this finite theory.

From what we have learned about the spectrum of this theory, there appear to be three natural directions for future investigations. One is to explore the fact that all these states seem to prefer a small valence number of adjoint fermions. We might consider a supersymmetric-like theory which only has adjoint fermions. Such a theory is obtained in 1+1 dimensions by simply dropping the boson terms in the supercharge [25,18]. One could try the same thing here. Alternatively, one can decouple the bosons by adding a mass term for them. These are two simple extensions of the present work that might avoid the large number of adjoint bosons in the bound states. The third alternative is to consider a Chern–Simons extension of this theory. This has the advantage of maintaining exact supersymmetry and giving the constituents a mass. In addition to these three directions for the $\mathcal{N} = 1$ theory, we can consider the next class of interesting models by adding more supersymmetry. The $\mathcal{N} = 2$ theory would be particularly interesting because it is the dimensional reduction of the $\mathcal{N} = 1$ theory in 3+1 dimensions.

ACKNOWLEDGMENTS

This work is supported in part by the US Department of Energy. J.R.H. thanks the Department of Physics of the Ohio State University for its hospitality during a visit there while this work was being completed.

REFERENCES

[1] N. Seiberg and E. Witten, Nucl. Phys. B **431**, 484 (1994).
[2] N. Seiberg, Nucl. Phys. B **435**, 129 (1995).
[3] J.M. Maldacena, Adv. Theor. Math. Phys. **2**, 231 (1998), hep-th/9711200.
[4] H.-C. Pauli and S.J. Brodsky, Phys. Rev. D **32**, 1993 (1985); **32**, 2001 (1985).
[5] S.J. Brodsky, H.-C. Pauli, and S.S. Pinsky, Phys. Rep. **301**, 299 (1998), hep-ph/9705477.
[6] Y. Matsumura, N. Sakai, and T. Sakai, Phys. Rev. D **52**, 2446 (1995).
[7] A. Hashimoto and I.R. Klebanov, Mod. Phys. Lett. A **10**, 2639 (1995).
[8] F. Antonuccio, O. Lunin, and S. Pinsky, Phys. Lett. B **429**, 327 (1998), hep-th/9803027.
[9] F. Antonuccio, O. Lunin, and S. Pinsky, Phys. Rev. D **58**, 085009 (1998), hep-th/9803170.
[10] F. Antonuccio, O. Lunin, H.-C. Pauli, S. Pinsky, and S. Tsujimaru, Phys. Rev. D **58**, 105024 (1998), hep-th/9806133.
[11] F. Antonuccio, H.-C. Pauli, S. Pinsky, and S. Tsujimaru, Phys. Rev. D **58**, 125006 (1998), hep-th/9808120.
[12] F. Antonuccio, O. Lunin, and S. Pinsky, Phys. Lett. B **442**, 173 (1998), hep-th/9809165.
[13] F. Antonuccio, O. Lunin, and S. Pinsky, Phys. Rev. D **59**, 085001 (1999), hep-th/9811083.
[14] P. Haney, J.R. Hiller, O. Lunin, S. Pinsky, and U. Trittmann, Phys. Rev. D **62**, 075002 (2000), hep-th/9911243.
[15] F. Antonuccio, A. Hashimoto, O. Lunin, and S. Pinsky, JHEP **9907**, 029 (1999), hep-th/9906087.
[16] J.R. Hiller, O. Lunin, S. Pinsky, and U. Trittmann, Phys. Lett. B **482**, 409 (2000), hep-th/0003249.
[17] S. Dalley and I. Klebanov, Phys. Rev. D **47**, 2517 (1993), hep-th/9209049.
[18] D. Kutasov, Nucl. Phys. B **414**, 33 (1994).
[19] T. Maskawa and K. Yamawaki, Prog. Theor. Phys. **56**, 270 (1976).
[20] F. Antonuccio, O. Lunin, S. Pinsky , and S. Tsujimaru, Phys. Rev. D **60**, 115006 (1999), hep-th/9811254.
[21] J.S. Rozowsky and C.B. Thorn. Phys. Rev. Lett. **85**, 1614 (2000), hep-th/0003301.
[22] E. Witten, in *The many faces of the superworld*, edited by M.A. Shifman, (World Scientific, Singapore, 2000), p. 156, hep-th/9903005.
[23] C. Lanczos, J. Res. Nat. Bur. Stand. **45**, 255 (1950); J.H. Wilkinson, *The Algebraic Eigenvalue Problem* (Clarendon, Oxford, 1965); B.N. Parlett, *The Symmetric Eigenvalue Problem* (Prentice–Hall, Englewood Cliffs, NJ, 1980); J. Cullum and R.A. Willoughby, J. Comput. Phys. **44**, 329 (1981); *Lanczos Algorithms for Large Symmetric Eigenvalue Computations* (Birkhauser, Boston, 1985), Vol. I and II; G.H. Golub and C.F. van Loan, *Matrix Computations* (Johns Hopkins University Press, Baltimore, 1983).
[24] J. Cullum and R.A. Willoughby, Ref. [23].
[25] F. Antonuccio and S. Pinsky, Phys. Lett. B **439**, 142 (1998), hep-th/9805188.
[26] D. Gross, A. Hashimoto, and I. Klebanov, Phys. Rev. D **57**, 6420 (1998), hep-th/9710240.